

Kinetic Energy Release in Fission of  $U^{238}$ ,  $U^{235}$ ,  $Th^{232}$ , and  $Bi^{209}$  by High Energy Neutrons

J. JUNGERMAN AND S. C. WRIGHT

*Radiation Laboratory, Department of Physics, University of California, Berkeley, California*

(Received June 6, 1949)

The ionization produced by single fission fragments was observed in an ionization chamber using electron collection. If fission is induced by 90-Mev neutrons, the distribution of kinetic energy of the fission fragment *versus* the number of fragments is found to have a single peak in contrast to the double-peaked curve corresponding to the fission made by thermal neutrons. Fission induced by 45-Mev neutrons gives a distribution in which two peaks appear. The dip between the two peaks is about twenty percent of the height of the peaks. The mean kinetic energy is found to be  $80 \pm 2$  Mev for  $U^{238}$ ,  $83 \pm 1.5$  Mev for  $U^{235}$ ,  $82 \pm 2$  Mev for  $Th^{232}$ , and  $71 \pm 2$  Mev for  $Bi^{209}$  in the case of fission produced by 90-Mev neutrons. The mean kinetic energy is  $79 \pm 3$  Mev for  $U^{238}$  and  $84 \pm 3$  Mev for  $Th^{232}$  if 45-Mev neutrons are used. The most probable kinetic energy of the fragment is 83 Mev for  $U^{238}$ , 80 Mev for  $U^{235}$ , 83 Mev for  $Th^{232}$ , and 75 Mev for  $Bi^{209}$  in the case of fission produced by 90-Mev neutrons. The bearing of these observations on the mechanism of fission is discussed.

## INTRODUCTION

THE kinetic energy release occurring in fission induced by low energy neutrons has been studied by Jentschke,<sup>1</sup> Flammersfeld *et al.*,<sup>2</sup> Brolley,<sup>3</sup> Deutsch and Ramsey,<sup>4</sup> and Fowler and Rosen.<sup>5</sup> The results of these experiments show that the distribution of the kinetic energy of single fragments *versus* the number of fragments consists of two peaks. The energy distribution is consistent with the mass distribution of the fragments known from chemical evidence and the assumption that the kinetic energy observed is derived only from the coulomb repulsion of two charged fragments.<sup>4</sup> The object of the experiment reported here was to investigate the kinetic energy distribution of single fragments produced in fission caused by 90-Mev and 45-Mev neutrons and the influence of the increased excitation on the mean fragment energy. To this aim the kinetic energy of single fragments was measured by the use of an ionization chamber, a linear amplifier, and a camera for photographically recording pulse heights on an oscilloscope.

## EXPERIMENTAL

Figure 1 shows a diagram of the ionization chamber employed. Each target plate had a foil spot welded to

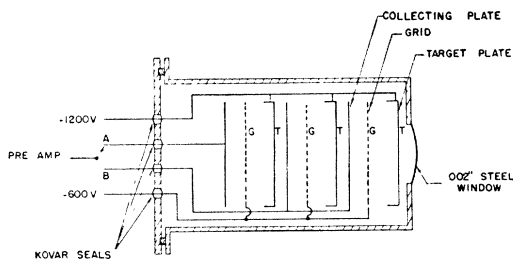


FIG. 1. Fission chamber.

- <sup>1</sup> W. Jentschke, *Zeits. f. Physik* **120**, 165 (1943).
- <sup>2</sup> A. Flammersfeld, *Zeits. f. Physik* **120**, 450 (1943).
- <sup>3</sup> J. E. Brolley, CN 1840.
- <sup>4</sup> M. Deutsch and Ramsey, LADC 257.
- <sup>5</sup> J. L. Fowler and L. Rosen, *Phys. Rev.* **72**, 926 (1947).

its surface. This foil was covered with the element under investigation. The foils in the cases of uranium and thorium were prepared by painting solutions of the nitrates on 1-mil aluminum and baking at  $500^\circ\text{C}$  until the oxides were formed.<sup>6</sup> The amount of material never exceeded  $3 \times 10^{-5}$  g/cm<sup>2</sup>. Foils surfaced with  $5 \times 10^{-5}$  g/cm<sup>2</sup> of bismuth were prepared by evaporation of the metal on 1-mil aluminum.

The grids *G* consisted of 3-mil nichrome wire 50 mils apart. The chamber was filled with pure argon at a pressure of 160 cm of Hg. The electrodes were so arranged that at this gas pressure the distance between the target plate *T* and the grid *G* was greater than the range of the fragments. The voltages were such that a stronger electric field existed between the grid and collecting plate than between the grid and the target plate. This tended to funnel the lines of force through the spaces in the grid and to prevent electrons from being collected at the grid.

Charged particles produced by the neutron beam in the chamber electrodes and gas caused spurious ionization pulses to be superimposed on the pulses from the fission fragments. In order to reduce this background ionization as much as possible, the chamber walls and electrodes were made as thin as practicable. The neutron beam entered through a 2-mil stainless steel window, traversed a 1-mil aluminum foil with the sample on it, the grid, and finally a 0.5-mil aluminum foil collecting plate. It then passed on through a similar unit of two plates and a grid. There were four such units in all. The last usually contained a sample of  $U^{235}$  for calibration purposes.

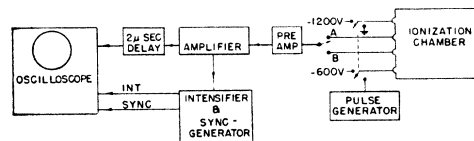


FIG. 2. Electronic circuit.

<sup>6</sup> T. Jorgensen, MDDC 467.

FIG. 3. Fission pulse.

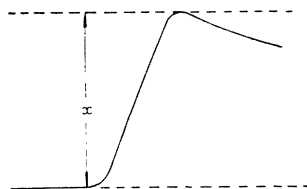
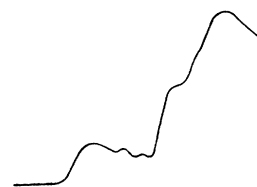


FIG. 4. Rejected fission pulse.



The electronic circuit is shown schematically in Fig. 2. This arrangement was employed in order to discriminate both electronically during the experiment and visually during the film analysis, against pulses caused by high energy neutron reactions in the argon and chamber plates along the path of the beam. A pulse from the ionization chamber was amplified and then fed directly onto the oscilloscope deflection plates via a 2- $\mu$ sec. delay line. Another amplifier output fed the pulse to the discriminator housed in the intensifier and sync-generator chassis. If the pulse was high enough to be accepted by the discriminator, an intensifying pulse traveled to the oscilloscope grid. At the same time the pulse initiated a 5- $\mu$ sec. sweep on the oscilloscope. In this way it was possible to see the start of the trace, the pulse rise, and the first part of the decay. Figure 3 shows the form of a typical pulse. The distance  $\alpha$  in the figure was taken to be the pulse height. Any pulse in which the initial base line and the pulse rise form differed from that in Fig. 3 was rejected. Figure 4 is an exaggerated example of such a rejected pulse. These unsatisfactory pulses were assumed to be due to a combination of fission fragment ionization and ionization produced by neutron reactions in the electrodes and gas. Their number never amounted to more than 5 percent of the total. The discriminator on the intensifier circuit prevented a large number of low energy pulses from being recorded. This considerably simplified the photographic analysis and made the readings more accurate. The amplifier was of the fast rise time variety stabilized by inverse feed back. The fission pulses had a rise time of 1.5- $\mu$ sec. and decayed to  $1/e$  in 10- $\mu$ sec. A fast rise time pulse generator connected when required to the grid of the chamber, checked the linearity and amplification of the equipment on the different bombardments. Calibration pulses from the pulse generator were used before and after each run.

The pulses on the Dumont 248 oscilloscope were photographed with a camera using continuously moving 35-mm Super XX film. All pulse heights were measured on the same microfilm viewer.

In order to check the resolution of the apparatus and to calibrate the energy scale, the usual experimental arrangement in the ionization chamber was to have a sample of  $U^{235}$  on plate *A* and samples of the element under investigation on plate *B* (see Fig. 1). Immediately before or after a cyclotron run, a fission fragment energy distribution was made with slow neutrons on  $U^{235}$  using the same chamber gas and the same setting of the amplifier and oscilloscope. The resolution of the

chamber was considered satisfactory if the  $U^{235}$  (slow  $n$ , fission) fragment energy distribution agreed with the curves of Deutsch and Ramsey<sup>4</sup> within statistics. The absolute energy scale was determined by comparison of the Deutsch and Ramsey  $U^{235}$  distribution (assumed correct) to the  $U^{235}$  (slow  $n$ , fission) curves obtained in this experiment. The latter were in turn used to obtain the energy scale for the high energy neutron fission fragment distributions. This energy scale was checked within experimental error by measuring the pulses produced in our apparatus by the  $\alpha$ -particles of  $U^{234}$ . Since the cyclotron magnetic field was different at the bombardment and calibration positions, a check of the effect of position on the amplification of the apparatus was made by making slow neutron runs at both locations. The pulse height average was found to be 3 percent higher at the bombardment position. This factor has been included in the energy scale calculation.

The high energy neutrons used in these experiments were formed by bombardment of a  $\frac{3}{8}$ -in. Be target with 190-Mev or 95-Mev deuterons. Serber<sup>7</sup> gives the theoretical energy distribution of the neutrons. According to him if the incident deuteron has 190 Mev, then the width at  $\frac{1}{2}$  maximum is 26 Mev. In the case of incident deuterons of 95 Mev, the width at  $\frac{1}{2}$  maximum is 19 Mev. The possibility of near thermal neutrons being present in the neutron beam was investigated by taking a cadmium difference with the  $U^{235}$  target. No effect was observed. This distribution has been checked experimentally in the course of n-p scattering experiments.<sup>8</sup> The most probable neutron energies in the two cases are 90 Mev and 45 Mev, respectively. This is the meaning of the terms 90-Mev and 45-Mev neutrons as used in this paper. Ra-Be enclosed in paraffin provided a thermal neutron source.

## RESULTS

Figures 5, 6, 7, 8, 9, and 10 show the actual histograms of the fragment energy distributions of  $U^{238}$ ,  $U^{235}$ ,  $Th^{232}$ , and  $Bi^{209}$ , obtained in the experiment. Figure 11 shows a typical slow neutron calibration histogram. Figures 12 and 13 show the probable distributions corresponding to these histograms. Each curve is normalized to 1000 pulses. In order to check that all pulses corresponding to 40 Mev or more were due to the active material, cyclotron runs were made with an aluminum blank of the same thickness, 1 mil, as that supporting the sample. These blank runs

<sup>7</sup> R. Serber, Phys. Rev. **72**, 1008 (1947).

<sup>8</sup> R. Serber, Phys. Rev. **75**, 326 (1949).

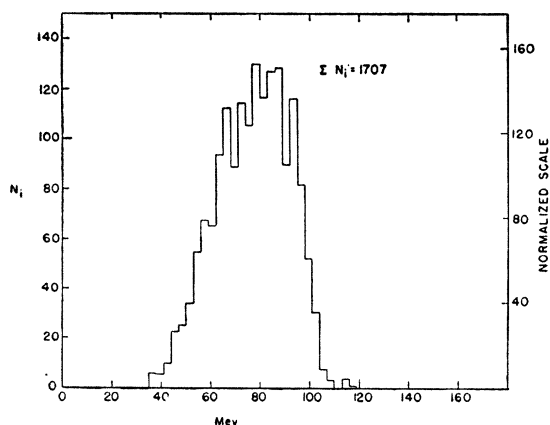


FIG. 5. Single fragment energy distribution  
90-Mev neutrons on  $U^{238}$ .

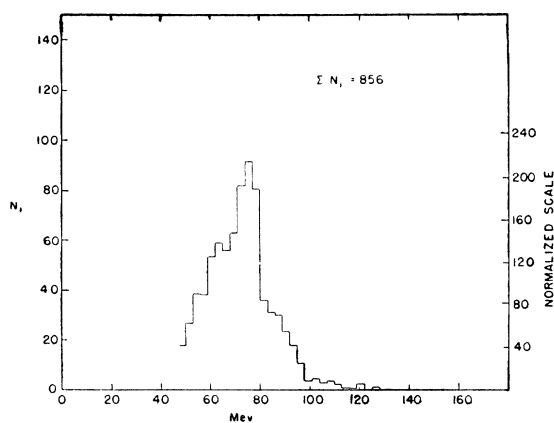


FIG. 8. Single fragment energy distribution  
90-Mev neutrons on Bi.

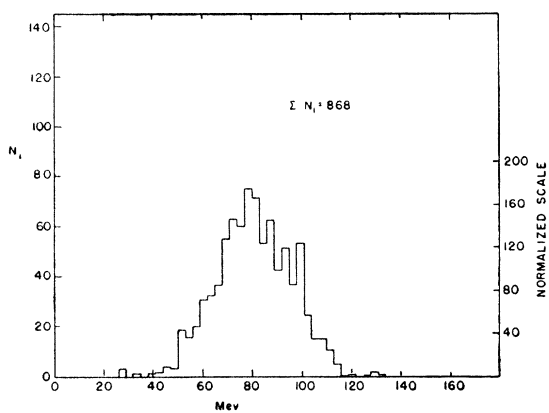


FIG. 6. Single fragment energy distribution  
90-Mev neutrons on  $U^{235}$ .

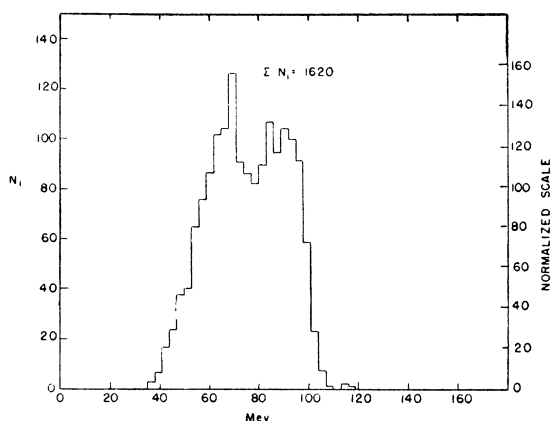


FIG. 9. Single fragment energy distribution  
45-Mev neutrons on  $U^{238}$ .

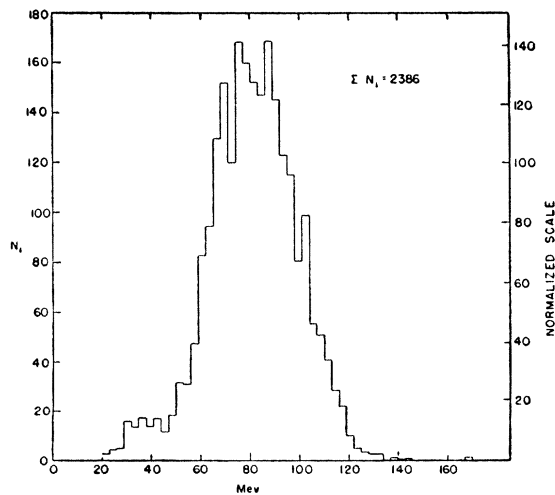


FIG. 7. Single fragment energy distribution  
90-Mev neutrons on Th.

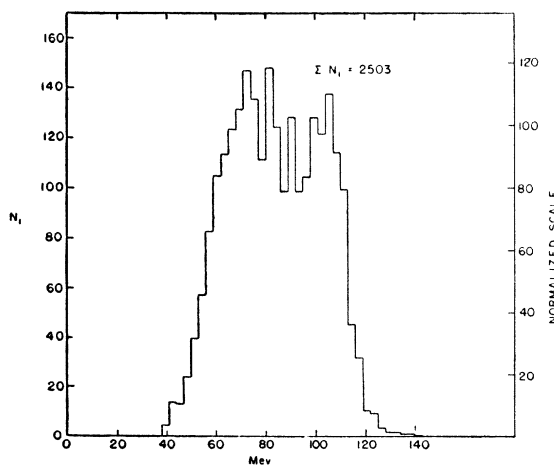


FIG. 10. Single fragment energy distribution  
45-Mev neutrons on  $Th^{232}$ .

showed that the number of pulses corresponding to fission fragments of 40 Mev or higher were negligible. For fission induced by 90-Mev neutrons it is found that

the mean fragment energy is  $80 \pm 2$  Mev for  $U^{238}$ ,  $83 \pm 1.5$  Mev for  $U^{235}$ ,  $82 \pm 2$  Mev for  $Th^{232}$ , and  $71 \pm 2$  Mev for  $Bi^{209}$ . The energy spread at one-half maximum

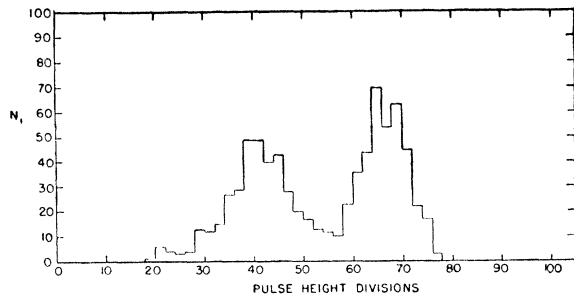


FIG. 11. Single fragment energy distribution slow neutrons on  $U^{238}$ .

is 40 Mev for  $U^{238}$ , 38 Mev for  $U^{235}$ , 44 Mev for  $Th^{232}$ , and 24 Mev for  $Bi^{209}$ . For fission induced by 45 Mev neutrons two peaks appeared in the energy distributions. For  $Th^{232}$  the maxima are at 73 Mev and 104 Mev, for  $U^{238}$  at 68 Mev and 89 Mev. The mean fragment energy is  $84 \pm 3$  Mev for  $Th^{232}$  and  $79 \pm 3$  Mev for  $U^{238}$ . The form of the distributions should be accurate within statistics.

#### DISCUSSION

The foregoing assumes that the number of ion pairs is proportional to the energy of the fission fragments producing them.

If the fission is assumed to be binary, as is most probable, this experiment shows that the mode of fission induced by 90-Mev neutrons that gives equal kinetic energies to the fragments is the most probable one in contrast to the results of thermal neutron fission. The mean kinetic energy of the fragments is, in the case of  $U^{235}$ , only 5-Mev higher than that from fission induced by slow neutrons. The kinetic energy of the incident neutron must therefore be accounted for by some other mechanism than appearance in the kinetic energy of the fission fragments.<sup>9</sup>

Goekermann and Perlman<sup>10</sup> have investigated fission products formed from bismuth by 200-Mev deuterons. They find that the mass-number distribution has a maximum at about 100-mass units. This indicates a loss of approximately 10 neutrons during the fission process.

The following mechanism is tentatively suggested for the fission process caused by high energy neutrons. The mechanism is shown schematically in Fig. 14. The compound nucleus  $Z^{A+1*}$  is formed from the nucleus  $Z^A$  by capture of a high energy neutron. This compound nucleus evaporates neutrons until fission can effectively compete with the neutron emission. The competition occurs until the energy  $A$  of the compound nucleus is less than the binding energy  $C$  of a neutron to the nucleus  $Z^{A+1-J}$ , where  $J$  is the number of neutrons

<sup>9</sup> According to M. L. Goldberger, Phys. Rev. **74**, 1269 (1948), the average excitation a nucleus receives from a collision with a 90-Mev neutron is appreciably less than 90 Mev.

<sup>10</sup> R. H. Goekermann and I. Perlman, Phys. Rev. **73**, 1127 (1948).

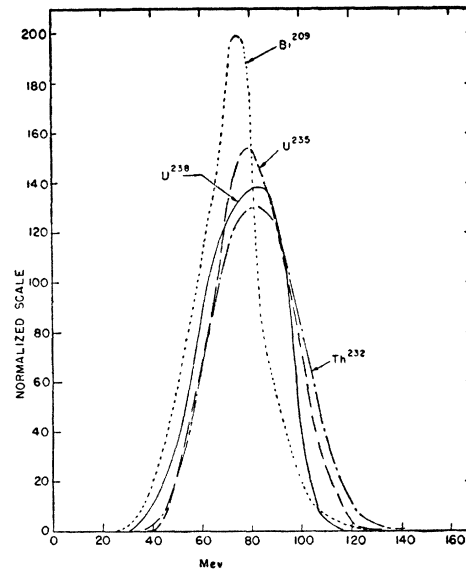


FIG. 12. Probable fragment energy distributions 90-Mev neutrons on  $U^{238}$ ,  $U^{235}$ ,  $Th^{232}$ , and  $Bi^{209}$ .

previously evaporated. Fission may be expected to have a threshold at some energy  $B$  above the ground level.

According to this picture the excess nuclear excitation is largely removed by neutron emission. It also predicts that the cross section for fission should be less than the total cross section with fluctuations from element to element. This is in agreement with the following. Recent measurements by Jungerman, Kelly, Wiegand, and Wright give the absolute fission cross section for 90-Mev neutrons on uranium and thorium to be 1.4 barns and 1.0 barns respectively. In each case the cross section is less than one half the geometric cross section and the two values differ considerably. There is no evidence at present concerning the time of neutron emission relative to the fission process.

In the high energy neutron fission of  $U^{235}$  the mean kinetic energy of the fragments is only slightly higher than that of the thermal neutron fission fragments. For

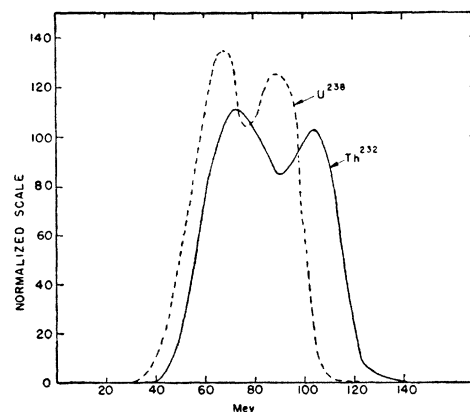


FIG. 13. Probable fragment energy distribution 45-Mev neutrons on  $U^{238}$  and  $Th^{232}$ .

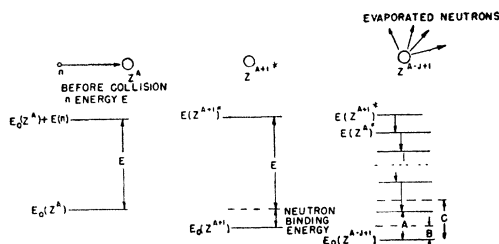


FIG. 14. Tentative fission mechanism.

Bi<sup>209</sup> the mean fragment energy is 0.91 times the latter. It was pointed out in the introduction that the energy distribution of the fragments in thermal neutron fission is consistent with their known mass distribution under the assumption that the kinetic energy observed is derived from the coulomb repulsion of two charged fragments. Since it has been suggested above that in high energy neutron fission the actual division of the nucleus only occurs in a relatively unexcited state, in fact of the same order of excitation as in the thermal neutron case, the high energy case should agree with a similar treatment. This can be easily checked for symmetrical fission with the crude model of Fig. 15. At the moment of separation the two fragments are assumed spherical in shape with a uniform distribution of charge and radii  $R = r_0 \times A^{1/3}$  where  $A$  is the mass number of the fragment and  $r_0$  is a constant. Also the charge of the fragments is assumed proportional to their mass. Under these conditions the coulomb potential energy  $E_c$  at the moment of separation will be

$$E_c = \frac{(Z_1 Z_2) e^2}{r_0 (A_1^{1/3} + A_2^{1/3})}$$

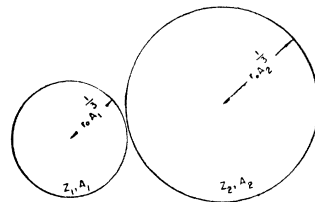


FIG. 15. Fission fragments at the moment of separation.

and for symmetrical fission

$$E_{c,s} = \frac{(Z_1 e)^2}{2r_0 (A_1)^{1/3}} = \frac{(Ze/2)^2}{2r_0 ((A+J-1)/2)^{1/3}}$$

Comparison of  $E_{c,s}$  for 90-Mev neutrons on Bi<sup>209</sup> and on U<sup>235</sup> and placing  $J$  equal to 10 gives the ratio 0.88 which agrees moderately well with the experimental value  $0.94 \pm 0.04$  considering the model used.

The fragment energy distributions obtained by the use of 45-Mev neutrons are interesting in that they exhibit the transition region between single and double peaked distributions characteristic of fission with 90 Mev and slow neutrons respectively. However, the actual energy distribution of the neutrons incident upon the fissionable material in this case has a width at half maximum of approximately 19 Mev so that it is impossible at present to say in what energy region the transition occurs.

#### ACKNOWLEDGMENTS

We wish to thank C. Wiegand for some electronic equipment and for many valuable suggestions during the course of this work. We are deeply indebted to Professor E. Segrè for suggesting this problem and for many stimulating discussions throughout the course of the investigation. Thanks are also due the 184-inch cyclotron crew for valuable cooperation.